Available online at www.sciencedirect.com
ScienceDirect
Trans. Nonferrous Met. Soc. China 25(2015) 3271−3278
Transactions of Nonferrous Metals Society of China
www.tnmsc.cn

Structure, morphology and opto-magnetic properties of Bi_2MoO_6 nano-photocatalyst synthesized by sol−gel method

V. UMAPATHY[1,2], A. MANIKANDAN[3], S. ARUL ANTONY[3], P. RAMU[4], P. NEERAJA[5]

1. Research and Development Centre, Bharathiar University, Coimbatore, Tamil Nadu 641 046, India;
2. Caplin Point Laboratories Limited, Chennai 600 017, India;
3. Postgraduate and Research Department of Chemistry, Presidency College, Chennai 600 005, India;
4. Department of Chemistry, Meenakshi Academy of Higher Education and Research, Chennai, Tamil Nadu 600 009, India;
5. Department of Chemistry, Adhiyamaan College of Engineering, Hosur, Tamil Nadu 635 109, India

Received 17 November 2014; accepted 23 March 2015

Abstract: Bismuth molybdate (Bi_2MoO_6) nano-particles (NPs) were synthesized using bismuth nitrate, ammonium molybdate, citric acid and ethyl cellulose by a simple sol−gel method. The structure, morphology, opto-magnetic and photocatalytic properties of the obtained powder were characterized by X-ray diffraction (XRD), Fourier transform infrared (FT-IR) spectra, high resolution scanning electron microscopy (HRSEM), energy dispersive X-ray (EDX), ultraviolet−visible diffuse reflectance spectra (DRS), photoluminescence (PL) spectra and vibrating sample magnetometer (VSM) techniques. The XRD, FT-IR and EDX results indicate that the resultant powder is pure and single phase crystalline Bi_2MoO_6 with orthorhombic structure. The HRSEM image shows that the morphology of obtained powder consists with well defined nano-particles structure. The VSM results show superparamagnetic behavior of the obtained nano-particles. The photocatalytic activity of Bi_2MoO_6 nano-particles was performed. The addition of TiO_2 catalyst enhances the photocatalytic activity of Bi_2MoO_6 nano-particles. The catalysts Bi_2MoO_6, TiO_2 and mixed oxide catalyst Bi_2MoO_6−TiO_2 nano-composites (NCs) were tested for the photocatalytic degradation (PCD) of 4-chlorophenol (4-CP). It is found that the PCD efficiency of Bi_2MoO_6−TiO_2 NCs is higher than that of pure Bi_2MoO_6 and TiO_2 catalysts.

Key words: Bi_2MoO_6; nanostructure; sol−gel synthesis; optical properties; magnetic properties; photocatalyst

1 Introduction

Nanostructured semiconductor materials have attracted considerable attention in nanoscience and nanotechnology, due to their unique physical−chemical properties compared with those of the same bulk materials [1]. Recently, metal molybdates materials have been widely used in photoluminescence, microwave applications, optical fibers, scintillator materials, humidity sensors and photocatalysis [2,3]. However, bismuth oxide, Bi_2MO_6 (M=W, Mo), nanomaterials are of special interest, due to their dielectric, ion-conductive, luminescent and catalytic properties [4,5]. The unique properties of nanomaterials are not only dependent on the compositions but also on both size and shapes of materials which are scientific interest in many practical and technological applications [6−8]. Nowadays, Bi_2MO_6 nonmaterial has been used as an excellent solar-energy-conversion material for water splitting and photocatalytic degradation of organic compounds [9−14]. Among many metal molybdates, bismuth molybdate (Bi_2MoO_6) is an important photocatalyst for the degradation of organic compounds.

Various methods have been used to prepare Bi_2MoO_6 nanostrutures, such as hydrothermal [15], solid-state reaction [16], co-precipitation [17] and amorphous complex precursor [18] methods. However, using the above conventional methods, the Bi_2MoO_6 nano-particles (NPs) were produced comparatively large in size with irregular morphology and inhomogeneous, because MoO_3 has a tendency to vaporize at high temperatures. In this study, Bi_2MoO_6 nano-particles were prepared by a simple sol−gel method using ethyl cellulose as the surfactant. Ethyl cellulose is a derivative of cellulose in which some of hydroxyl groups on the

Corresponding author: P. NEERAJA; Tel: +91-9487819133; E-mail: researchneeraja@gmail.com
DOI: 10.1016/S1003-6326(15)63948-6

repeating glucose units are converted into ethyl ether groups. The number of ethyl groups can vary depending on the manufacturer. Ethyl cellulose contains hydroxyl group in its individual unit, which plays an important role in the dispersion process of Bi_2MoO_6 particles. This hydroxyl group forms an ester linkage with citric acid, which forms big polymeric structure that traps the metal oxides and water molecules and thus prevents the agglomeration of particles. The remarkable advantage of sol−gel method over the above method is the simplicity of the preparation procedure. Sol−gel method exhibits many advantages, such as low process temperature and high control of pure products.

Nanostructured photocatalyst materials have gained much interest, due to their potential application in environmental purification [11,19], solar energy conversion [20] and H_2 production by water splitting [9]. Recently, many studies have been carried out to exploit new visible light-driven photocatalysts. The photocatalytic activities of Bi_2WO_6 have been revealed by KUDO and HIJII [9], TANG et al [21] and ZHANG and ZHU [22]. KUDO et al [23,24] found out that Bi_2MoO_6 was able to carry out the photocatalytic O^{2-} evolution under visible light irradiation. The photocatalysis offers superior technology for the removal of different toxic organic compounds from water by using TiO_2 catalyst, which has been widely studied [25], because of its financial/economic and ecologically safe opportunity for solving the energy and pollution problems [26]. TiO_2 is an excellent photocatalyst, because of its high activity, low cost and good stability. In addition to TiO_2, other nanosized mixed oxides, such as tantalates [27,28], vanadates [29,30] and tungstates [11,19,31−34], have been reported for ultraviolet (UV) and visible light photocatalytic activities by many researchers.

Bi_2MoO_6 is an excellent material with visible light-driven photocatalytic activity for water splitting and decomposition of organic pollutants [35]. The improvement of photocatalytic activity of Bi_2MoO_6 can be achieved by doping with TiO_2 catalyst in order to reduce the charge carrier recombination. Such advanced Bi_2MoO_6−TiO_2 mixed catalyst extends its application through the generation of new catalytic sites, due to a strong interaction between them. Therefore, it is highly interesting and desirable to study the photocatalytic activity of Bi_2MoO_6−TiO_2 mixed oxide. HANKARE et al [36] have reported $ZnFe_2O_4$, TiO_2−$ZnFe_2O_4$, TiO_2−Al_2O_3−$ZnFe_2O_4$ photocatalysts for the degradation of methyl red and thymol blue. In this study, Bi_2MoO_6 nano-particles prepared by a simple sol−gel method. It was observed that Bi_2MoO_6 nano-particle can be used as a photocatalyst for the efficient bleaching and mineralization of 4-chloro phenol (4-CP) under visible light irradiation.

2 Experimental

2.1 Materials and methods

All the chemicals were of analytical grade obtained from Merck, India, and were used as received without further purification. Ammonium molybdate ($(NH_4)_6Mo_7O_{24}\cdot 4H_2O$), bismuth nitrate ($Bi(NO_3)_3\cdot 5H_2O$), citric acid and ethyl cellulose were used as the raw materials. Ethyl cellulose powders were sprinkled slowly into deionized water under continuous stirring to avoid the clumping of material in water. Bismuth nitrate and ammonium molybdate in stoichiometric ratio and citric acid were dissolved in deionized water separately. These solutions were added to ethyl cellulose solution at 50 °C to form sol. This sol is then heated slowly to 90 °C under constant stirring to obtain a wet gel. Then, the gel product was calcined at 650 °C for 2 h. It was ground in a mortar to form a final product of fine powder.

2.2 Characterization techniques

The characterizations of the obtained Bi_2MoO_6 nano-powder were conducted using various techniques to verify the phase formation, crystallite size, distribution and to explore other parameters of interest. The structural characterization of Bi_2MoO_6 nano-particles was performed using Rigaku Ultima X-ray diffractometer equipped with Cu K_α radiation (λ=1.5418 Å). The surface functional groups were analyzed by Perkin Elmer Fourier transform infrared (FT-IR) spectrometer. The morphological studies and energy dispersive X-ray analysis (EDX) of Bi_2MoO_6 NPs have been performed with a Jeol JSM6360 high resolution scanning electron microscope (HRSEM). The UV−visible diffuse reflectance spectrum (DRS) was recorded using Cary100 UV−visible spectrophotometer to estimate their band gap energy (E_g). The photoluminescence (PL) properties were recorded at room temperature using Varian Cary Eclipse Fluorescence Spectrophotometer. The magnetic measurements were carried out at room temperature using a PMC MicroMag 3900 model vibrating sample magnetometer equipped with 1 T magnet.

2.3 Photocatalytic reactor setup and degradation procedure

All photochemical reactions under identical conditions were carried out in a self-designed photocatalytic reactor. This model consists of eight medium pressure mercury vapor lamps (8 W) setting in parallel and emitting wavelength of 365 nm. It has a reaction chamber with specially designed reflectors made of highly polished Al and built in cooling fan at the bottom and black cover to prevent UV leakage. It is

provided with the magnetic stirrer at the center. The open borosilicate glass tube of 40 cm in height and 12.6 mm in diameter was used as a reaction vessel. The irradiation was carried out using only six parallel medium pressure mercury lamps. The solution was aerated continuously by a pump to provide oxygen and for the complete mixing of solution. Prior to the photocatalytic experiments, the adsorption of 4-CP on Bi_2MoO_6 and TiO_2-supported Bi_2MoO_6 nano-photocatalyst was carried out by mixing 100 mL aqueous solution of 4-CP with fixed mass of the respective photocatalyst. A known amount of commercial TiO_2 (Degussa P-25) was added to a known amount of Bi_2MoO_6 and finely ground in a mortar and pestle for 30 min so as to obtain a mixture of Bi_2MoO_6−TiO_2 in the required mole fraction. The photocatalytic degradation (PCD) was carried out by mixing 100 mL aqueous solution of 4-CP and fixed mass of Bi_2MoO_6 nano-photocatalyst. The PCD of 4-CP was also carried out with Bi_2MoO_6−TiO_2 mixed oxide. Therefore, the interactions of Bi_2MoO_6 with TiO_2 can be assumed to take place at the grain boundaries. The PCD efficiency was also calculated for pure oxides (Bi_2MoO_6 and TiO_2) and mixed oxide (Bi_2MoO_6−TiO_2). All solutions prior to photolysis were kept in dark by covering with Al foil to prevent any photochemical reactions. The PCD efficiency (η) was calculated from the following expression:

$$\eta=(C_i-C_t)/C_i\times100\% \quad (1)$$

where C_i is the initial concentration of 4-CP, C_t is the concentration of 4-CP after time t (min).

3 Results and discussion

3.1 Powder X-ray diffraction (XRD)

The crystal structure and phase analysis of the samples were characterized by powder X-ray diffraction (XRD) pattern. The XRD pattern of as-synthesized Bi_2MoO_6 powder shown in Fig. 1 is indexed to orthorhombic Bi_2MoO_6 according to the JCPDS database No. 21-0102 [15,37]. No impurities of secondary phases such as Bi_2O_3, MoO_3, and others were detected in the XRD pattern of product. The very high peak intensity suggests that the material is highly crystalline. This indicates the complete transformation of the precursor into orthorhombic Bi_2MoO_6 phase. The average crystallite size of Bi_2MoO_6 sample was calculated using Debye Scherrer formula given in Eq. (2):

$$L=\frac{0.89\lambda}{\beta\cos\theta} \quad (2)$$

where L is the crystallite size, λ is the X-ray wavelength, θ is the Bragg diffraction angle and β is the full width at half maximum (FWHM). The average crystallite size L calculated from the diffraction peaks is found to be 35−38 nm.

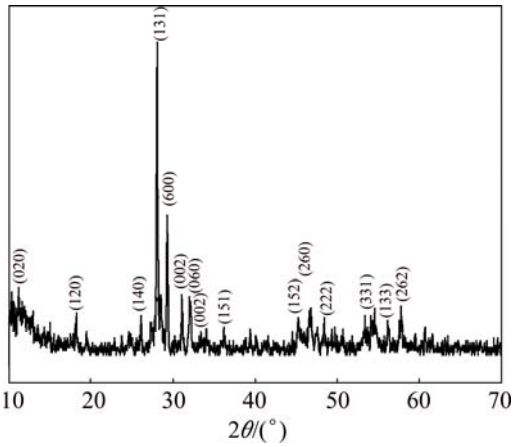

Fig. 1 XRD pattern of Bi_2MoO_6 NPs

The lattice parameter of the sample was calculated using the formula given in Eq. (3):

$$\sin^2\theta=\frac{\lambda^2}{4a^2}h^2+\frac{\lambda^2}{4b^2}k^2+\frac{\lambda^2}{4c^2}l^2 \quad (3)$$

where h, k and l are Miller's indices. The calculated lattice parameters are found to be a=5.498 Å, b=16.118 Å, and c=5.401 Å, which are in good agreement with the JCPDS file card No. 21−0102. Similar values (a=5.502 Å, b=16.210 Å, and c=5.483 Å) have been reported earlier by ADHIKARI et al [37].

3.2 FT-IR spectral analysis

Figure 2 shows the Fourier transform infrared (FT-IR) spectrum of Bi_2MoO_6 nano-powders. The FT-IR spectrum contains a broad band between ~3200 and ~3500 cm^{-1} which is due to the hydroxyl (O—H) stretching mode [38]. A weak band appearing at 2137 cm^{-1} may be due to the combination band of C—H or O—H stretching. However, a sharp band at 1646 cm^{-1} is due to the presence of O—H bending vibration of water molecule. The spectrum of Bi_2MoO_6 sample shows absorption bands between ~650 and 850 cm^{-1} which is mainly due to Mo═O stretching vibration. However, the peak appearing at 720 cm^{-1} is ascribed to Mo(VI)—O tetrahedral stretching and the peak at 499 cm^{-1} corresponds to Bi(III)—O octahedral stretching vibration.

3.3 Scanning electron microscopy (SEM) studies

The surface morphology of Bi_2MoO_6 sample was examined by high resolution scanning electron microscopy (HRSEM). Figure 3(a) shows the HRSEM image of Bi_2MoO_6 sample which consists of agglomerated particle-like nanostructure. The formation of agglomerated particle-like nanostructure may be due

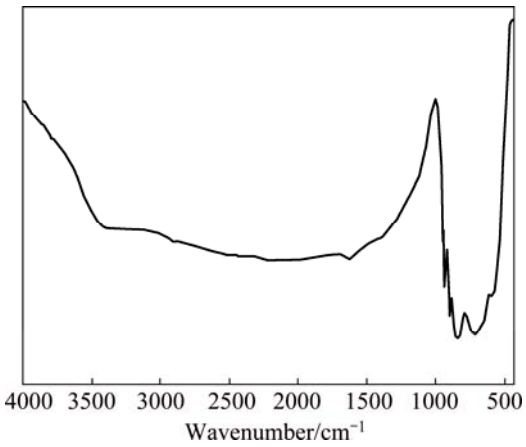

Fig. 2 FT-IR spectrum of Bi_2MoO_6 NPs

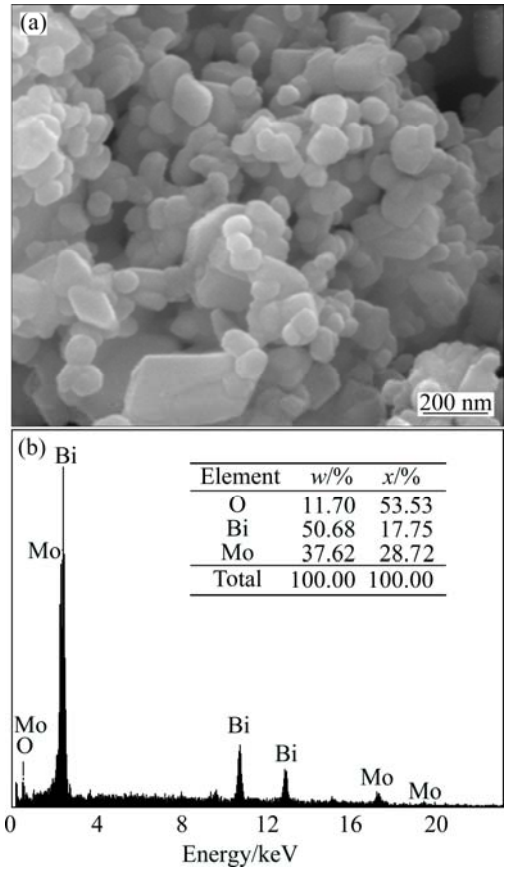

Element	w/%	x/%
O	11.70	53.53
Bi	50.68	17.75
Mo	37.62	28.72
Total	100.00	100.00

Fig. 3 HRSEM image (a) and EDX spectrum (b) of Bi_2MoO_6 NPs

to the attachment of magnetic nature of nano-crystals. The elemental composition and purity of Bi_2MoO_6 sample were also analyzed by energy dispersive X-ray (EDX) analysis. Figure 3(b) shows the EDX spectrum of Bi_2MoO_6 sample which shows the presence of Bi, Mo and O by the appearance of Bi, Mo and O peaks without any other characteristic peaks. Hence, the EDX results are perfect evidences to propose that the prepared sample does not contain any other elements and is indeed free from other impurities.

3.4 Optical properties

UV−visible absorption spectroscopy is an important technique for characterizing the optical properties of as-prepared Bi_2MoO_6 nano-powders. The UV−visible diffuse reflectance spectrum (DRS) of Bi_2MoO_6 nano-particle is shown in Fig. 4(a). The broad absorption band centered at 230 nm is attributed to the O^{2-} to Mo^{6+} charge transfer of the isolated MoO_6 sites [39]. The steep shape of DRS spectrum indicates that the visible light absorption is arisen from the band-gap transition instead of impurity levels [24,40]. The color of Bi_2MoO_6 sample is yellow, in accordance with the extension of its absorption edge to 478 nm. The steep absorption edge is at 478 nm, corresponding to a band gap energy E_g of about 2.59 eV (the inset in Fig. 4(a)), indicating that the sample exhibits an intense absorption in the visible light range. The DRS analysis was used to study the relation of crystallite size and band gap of the semiconductors. The band gap energy (E_g) of the samples can be evaluated using the Kubelka−Munk model. It allows the calculation of the absorption coefficient (α) by the measurement of the UV−visible diffuse reflectance. The kubelka−Munk function, $F(R)$, is directly proportional to the absorption coefficient (α) and the value is estimated from the following equation [41]:

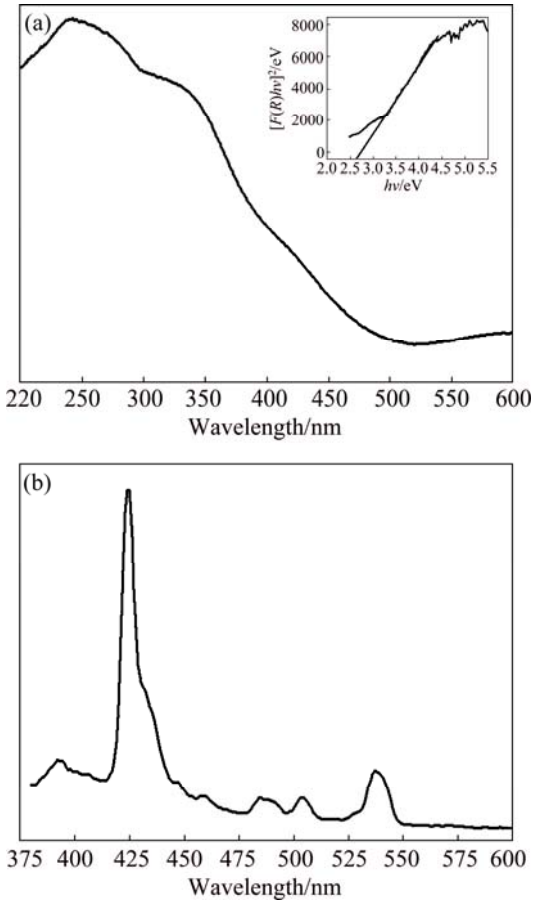

Fig. 4 UV−visible diffuse reflectance spectrum (a) and PL spectrum (b) of Bi_2MoO_6 NPs

$$F(R)=\alpha=\frac{(1-R)^2}{2R} \quad (4)$$

where α is the absorbance, R is the reflectance. A graph is plotted between $[F(R)h\upsilon]^2$ and $h\upsilon$, and the obtained intercept value is the band gap energy of the sample, as shown in the inset in Fig. 4(a). The estimated band gap value of Bi_2MoO_6 sample is 2.59 eV. The E_g of 2.59 eV is much closer to 2.53 eV [13], 2.60 eV [42] and 2.58 eV [43], for which the samples were synthesized by conventional/ microwave-assisted solvothermal, molten salt route and citrate method, respectively. Therefore, the observed different band gaps by different preparation routes could not result from the quantum-size effect, but can be ascribed to their different degrees of crystallization [18,34].

However, the color of the sample is light yellow and it is suggested that the visible light absorption is due to the transition from the valence band consisting of O 2p orbitals to the conduction band derived from the primary Mo 4d orbitals in MoO_6 octahedra and the secondary Bi 6p orbitals [24].

The room temperature photoluminescence (PL) spectrum of Bi_2MoO_6 nano-particles is shown in Fig. 4(b). The PL spectrum was recorded in order to study the defects and other impurity states of semiconductors. The PL spectrum shows an emission band in the UV region at around 385 nm, which is attributed to the near band-edge emission of Bi_2MoO_6, indicating the quantum confinement effect [44−46]. However, the luminescence peaks were observed in the visible region at around 422, 458, 485, 510 and 535 nm, which are mainly due to the presence of radiative defects and oxygen vacancies of Bi_2MoO_6 nano-particles.

3.5 Magnetic properties

Figure 5 shows the magnetic hysteresis (M−H) loop of Bi_2MoO_6 nano-particles with the field sweeping from −15 to +15 kA/m at room temperature. The obtained Bi_2MoO_6 nano-particles show superparamagnetic behavior. The Bi_2MoO_6 nano-particles are important magnetic materials. The Bi_2MoO_6 nano-particles obtained by sol−gel method show remarkable super-paramagnetic behavior with relatively high saturation magnetization (M_s) than those obtained by other methods, which may be due to the synthesis route and conditions, the type of precursors, calcinations, etc. The saturation magnetization (M_s), remnant magnetization (M_r) and coercivity (H_c) values of the sample Bi_2MoO_6 are 2.55×10^{-4} A·m^2/kg, 0.44×10^{-4} A·m^2/kg and 142.57 kA/m, respectively. However, the magnetic properties of materials are influenced by many factors, such as size, crystallinity and surface structure.

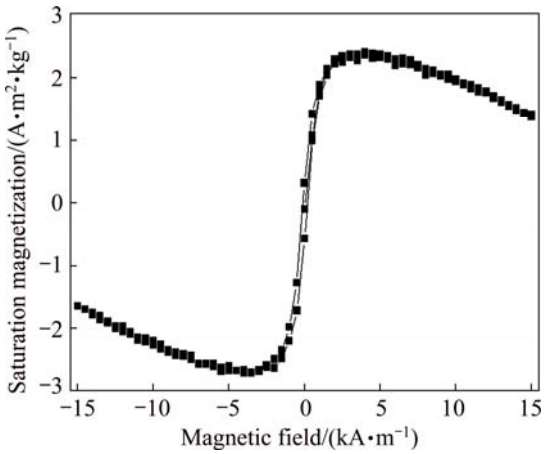

Fig. 5 Magnetic hysteresis (M−H) loops of Bi_2MoO_6 NPs

3.6 Photocatalytic properties

It has been generally accepted that the crystallinity, size, shape and morphologies of the nano-materials are important factors that influence their photocatalytic activity. It is important to prepare Bi_2MoO_6 nano-photocatalyst to understand the catalytic activity of TiO_2 catalyst supported Bi_2MoO_6−TiO_2 nano-composites. This study made an attempt to reveal the relationship between optical and photocatalytic properties of pure metal oxides (Bi_2MoO_6 and TiO_2) or mixed metal oxide (Bi_2MoO_6−TiO_2) and a series of experiments were carried out with 4-CP in aqueous suspension with the light wavelength of 365 nm.

The effect of TiO_2-supported Bi_2MoO_6 nano-photocatalyst on the PCD efficiency was evaluated, as shown in Fig. 6. The control experiment was carried out in the absence of catalyst by irradiating the solution with UV radiation (photolysis). The degradation of 4-CP due to photolysis is found to be less than 10%. The PCD efficiency of Bi_2MoO_6 is low when compared with that of TiO_2. The PCD efficiency of TiO_2-supported Bi_2MoO_6 (i.e., Bi_2MoO_6−TiO_2) photocatalyst is higher than that of pure Bi_2MoO_6 photocatalyst. It is found that the photocatalytic activity of single phase Bi_2MoO_6 is enhanced when it is coupled with TiO_2 catalyst to form a composite catalyst [47, 48]. Though, the band gap of Bi_2MoO_6 is smaller (2.59 eV) than that of TiO_2 (3.2 eV) and it is a visible light active catalyst, which exhibits lower photocatalytic activity, due to its lower valence band potential compared with that of TiO_2 [36]. When TiO_2 and Bi_2MoO_6 are coupled and irradiated with UV−visible light, the photocatalytic activity is improved, though the charge carriers can migrate to Bi_2MoO_6 due to higher valence band potential of TiO_2. The 4-CP photocatalytic degradation occurs by the hydroxyl radicals attacking the phenyl groups of 4-CP. It is believed to be initiated through the attacks by hydroxyl radicals at the phenyl groups of 4-CP, which may result

in the formation of intermediates that may be mono-hydroxylated or dihydroxylated 4-CP and followed by the cleavage of two phenyl groups into intermediates. In addition, hydroquinone is the major intermediate.

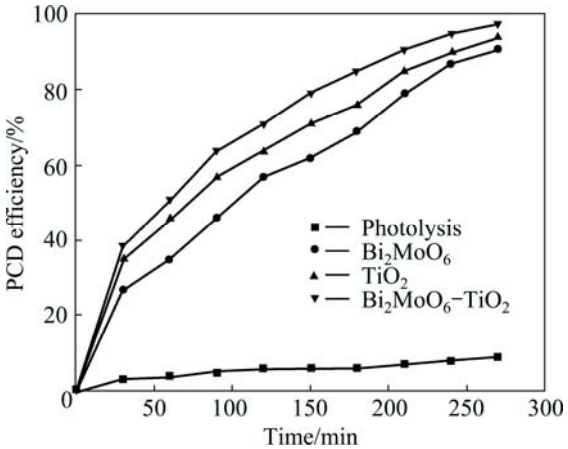

Fig. 6 PCD efficiency of TiO_2-supported Bi_2MoO_6 photocatalyst (concentrations of 4-CP and photocatalyst 200 and 300 mg/L, respectively; light wavelength 365 nm; pH value 8)

The photo-degradation kinetics of 4-CP with and without Bi_2MoO_6−TiO_2 nano-photocatalyst in the presence of UV light was evaluated using the pseudo first-order rate equation:

$$\ln(C_t/C_o)=-k_1t \quad (5)$$

where C_o is the initial concentration (mg/L), C_t is the concentration (mg/L) at time t, t is the UV light exposure time and k_1 is the first-order rate constant. The values of k_1 in relation to 4-CP concentrations of 50 mg/L and 1000 mg/L in the presence of Bi_2MoO_6−TiO_2 catalyst are 1.67×10^{-2} and 0.79×10^{-2} min^{-1}, respectively, whereas the values of k_1 of the same reaction without catalyst are found to be 0.63×10^{-2} and 0.29×10^{-2} min^{-1}, respectively. Higher rate constant achieved using Bi_2MoO_6−TiO_2 catalyst can be attributed to the combined effects of the adsorption of 4-CP molecule over catalyst surface followed by oxidation using the generated hydroxyl radicals and the direct attack of photo-generated holes [49].

4 Conclusions

1) Bi_2MoO_6 nano-particles were synthesized via a simple sol−gel method using ethyl cellulose as the surfactant. The XRD results indicate pure single phase crystalline with orthorhombic structure of Bi_2MoO_6. The HRSEM image shows that the morphology of the product consists with well defined nano-particles structure with agglomeration.

2) The VSM results show superparamagnetic behavior. The PCD efficiency of Bi_2MoO_6 is low when compared with that of TiO_2 catalyst. The PCD efficiency of TiO_2-supported Bi_2MoO_6 (i.e., Bi_2MoO_6−TiO_2) photocatalyst is higher than that of pure Bi_2MoO_6 photocatalyst. These results indicate that Bi_2MoO_6–TiO_2 nanostructures may find applications in water pollution control.

3) Compared with other synthetic methods, sol−gel method is a facile, low-cost pathway to prepare novel Bi_2MoO_6 nano-architectures.

4) The orthorhombic Bi_2MoO_6 and Bi_2MoO_6−TiO_2 nano-photacatalysts show photocatalytic efficiencies of 91.64% and 97.02%, respectively, for the degradation of 4-CP under the UV−visible light irradiation.

References

[1] ABDULLAH A, SALEEMI A S, REHMAN M A. Comparative study of nano crystalline ceria synthesized by different wet-chemical methods [J]. Journal of Superconductivity and Novel Magnetism, 2014, 27: 273−276.

[2] KARAOGLU E, BAYKAL A. $CoFe_2O_4$–Pd(0) nanocomposite: Magnetically recyclable catalyst [J]. Journal of Superconductivity and Novel Magnetism, 2014, 27: 2041−2047.

[3] LIYAN W, HONGXIA W, AIJIE W, MIN L. Surface modification of a magnetic SiO_2 support and immobilization of a nano-TiO_2 photocatalyst on it [J]. Chinese Journal of Catalysis, 2009, 30: 939−944.

[4] BAUX N, VANNIER R N, MAIRESSE G, NOWOGROCKI G. Oxide ion conductivity in $Bi_2W_{1-x}ME_xO_{6-x/2}$ (ME=Nb, Ta) [J]. Solid State Ionics, 1996, 91: 243−248.

[5] ISLAM M S, LAZURE S, VANNIER R N, NOWOGROCKI G. MAIRESSE, G. Structural and computational studies of Bi_2WO_6 based oxygen-ion conductors [J]. Journal of Materials Chemistry, 1998, 8: 655−660.

[6] LU L, KOBAYASHI A, TAWA K, OZAKI Y. Silver nano particles with special shapes: Controlled synthesis and their surface plasmonresonance and surface-enhanced Raman scattering [J]. Chemistry of Materials, 2006, 18: 4894−4901.

[7] YU J Q, KUDO A. Effects of structural variation on the photocatalytic performance of hydrothermally synthesized $BiVO_4$ [J]. Advanced Functional Materials, 2006, 16: 2163−2169.

[8] ZHANG L S, LI J L, CHEN Z G, TANG Y W, YU Y. Preparation of Fenton reagent with H_2O_2 generated by solar light-illuminated nano-Cu_2O/MWNTs composites [J]. Applied Catalysis A, 2006, 299: 292−297.

[9] KUDO A, HIJII S. H_2 or O_2 evolution from aqueous solutions on layered oxide photocatalysts consisting of Bi^{3+} with $6s^2$ configuration and d^0 transition metal ions [J]. Chemistry Letters, 1999, 28(10): 1103−1104.

[10] TANG J W, ZOU Z G, YE J H. Photocatalytic decomposition of organic contaminants by Bi_2WO_6 under visible light irradiation [J]. Catalysis Letter, 2004, 92: 53−56.

[11] FU H, PAN C, YAO W, ZHU Y. Visible-light-induced degradation of rhodamine B by nanosized Bi_2WO_6 [J]. Journal of Physical Chemistry B, 2005, 109: 22432−22439.

[12] YU J G, XIONG J F, CHENG B, YU Y, WANG J B. Hydrothermal preparation and visible-light photocatalytic activity of Bi_2WO_6 powders [J]. Journal of Solid State Chemistry, 2005, 178: 1968−1972.

[13] BI J H, WU L, LI J, LI Z H, WANG X X, FU X Z. Simple

solvothermal routes to synthesize nanocrystalline Bi_2MoO_6 photocatalysts with different morphologies[J]. Acta Materialia, 2007, 55: 4699−4705.

[14] ZHANG L S, WANG W Z, ZHOU L, XU H L. Bi_2WO_6 nano- and microstructures: Shape control and associated visible-light-driven photocatalytic activities [J]. Small, 2007, 3: 1618−1625.

[15] ZHAO X, XU T, YAO W, ZHU Y. Photodegradation of dye pollutants catalyzed by γ-Bi_2MoO_6 nanoplate under visible light irradiation [J]. Applied Surface Science, 2009, 255: 8036−8040.

[16] ZHAO X, QU J H, LIU H J, HU C. Photoelectrocatalytic degradation of triazine containing azo dyes at g-Bi_2MoO_6 film electrode under visible light irradiation (l>420 nm) [J]. Applied Catalysis B: Environmental, 2007, 41: 6802−6807.

[17] HIPOLITO E L, CRUZ A M, YU Q L, BROUWERS H J H. Photocatalytic removal of nitric oxide by $Bi_2Mo_3O_{12}$ prepared by co-precipitation method [J]. Applied Catalysis A: General, 2013, 468: 322−326.

[18] MAN Y, ZONG R, ZHU Y. Preparation and photoelectrochemical properties of Bi_2MoO_6 films [J]. Acta Physico-Chimica Sinica, 2007, 23: 1671−1676.

[19] ZHANG S C, ZHANG C, MAN Y, ZHU Y F. Visible-light-driven photocatalyst of Bi_2WO_6 nanoparticles prepared via amorphous complex precursor and photocatalytic properties [J]. Journal of Solid State Chemistry, 2006, 179: 62−69.

[20] ZHANG S C, YAO W Q, ZHU Y F, SHI L Y. Preparation and photoelectrochemical properties of Bi_2WO_6 films with visible light response [J]. Acta Physico-Chimica Sinica, 2007, 23: 111−115.

[21] TANG J W, ZOU Z G, YE J H. Photocatalytic decomposition of organic contaminants by Bi_2WO_6 under visible light irradiation [J]. Catalysis Letters, 2004, 92: 53−56.

[22] ZHANG C, ZHU Y F. Synthesis of square Bi_2WO_6 nanoplates as high-activity visible-light-driven photocatalysts [J]. Chemistry of Materials, 2005, 17: 3537−3545.

[23] YU J Q, KUDO A. Hydrothermal synthesis and photocatalytic property of 2-dimensional bismuth molybdate nanoplates [J]. Chemistry Letters, 2005, 34: 1528−1529.

[24] SHIMODAIRA Y, KATO H, KOBAYASHI H, KUDO A. Photophysical properties and photocatalytic activities of bismuth molybdates under visible light irradiation [J]. Journal of Physical Chemistry B, 2006, 110: 17790−17797.

[25] OLLIS D F, PELIZZETTI E, SERPONE N. Photocatalyzed destruction of water contaminants [J]. Environmental Science and Technology, 1991, 25: 1522−1529.

[26] HOFFMANN M R, MARTIN S T, CHOI W Y, BAHNEMANN D W. Environmental applications of semiconductor photocatalysis [J]. Chemical Reviews, 1995, 95: 69−96.

[27] HE Y, ZHU Y F, WU N Z. Synthesis of nanosized $NaTaO_3$ in low temperature and its photocatalytic performance [J]. Journal of Solid State Chemistry, 2004, 177: 3868−3872.

[28] XU T G, ZHAO X, ZHU Y F. Synthesis of hexagonal $BaTa_2O_6$ nanorods and influence of defects on the photocatalytic activity [J]. Journal of Physical Chemistry B, 2006, 110: 25825−25832.

[29] ZHANG S C, ZHANG C, YANG H P, ZHU Y F. Formation and performances of porous $InVO_4$ films [J]. Journal of Solid State Chemistry, 2006, 179: 873−883.

[30] ZHANG L W, FU H B, ZHANG C, ZHU Y F. Synthesis, characterization, and photocatalytic properties of $InVO_4$ nanoparticles [J]. Journal of Solid State Chemistry, 2006, 179: 804−811.

[31] FU H B, ZHANG L W, YAO W Q, ZHU Y F. Photocatalytic properties of nanosized Bi_2WO_6 catalysts synthesized via a hydrothermal process [J]. Applied Catalysis B: Environmental, 2006, 66: 100−110.

[32] ZHAO X, XU T G, YAO W Q, ZHANG C, ZHU Y F. Photoelectrocatalytic degradation of 4-chlorophenol at Bi_2WO_6 nanoflake film electrode under visible light irradiation [J]. Applied Catalysis B: Environmental, 2007, 72: 92−97.

[33] HUANG G L, ZHANG C, ZHU Y F. $ZnWO_4$ photocatalyst with high activity for degradation of organic contaminants [J]. Journal of Alloys and Compounds, 2007, 432: 269−276.

[34] ZHAO X, YAO W Q, WU Y, ZHANG S C, YANG H P, ZHU Y F. Fabrication and photoelectrochemical properties of porous $ZnWO_4$ film [J]. Journal of Solid State Chemistry, 2006, 179: 2562−2570.

[35] BI J, CHE J, WU L, LIU M. Effects of the solvent on the structure, morphology and photocatalytic properties of Bi_2MoO_6 in the solvothermal process [J]. Materials Research Bulletin, 2013, 48: 2071−2075.

[36] HANKARE P P, PATIL R P, JADHAV A V, GARADKAR K M, SASIKALA R. Enhanced photocatalytic degradation of methyl red and thymol blue using titania−alumina−zinc ferrite nanocomposite [J]. Applied Catalysis B: Environmental, 2011, 107: 333−339.

[37] ADHIKARI R, JOSHI B, GARCIA R N, ROSA E D, LEE S W. Microwave hydrothermal synthesis and infrared to visible upconversion luminescence of Er^{3+}/Yb^{3+} co-doped bismuth molybdate nanopowder [J]. Journal of Luminescence, 2014, 145: 866−871.

[38] TSAY J, FANG T. Effects of molar ratio of citric acid to cations and of pH value on the formation and thermal-decomposition behavior of barium titanium citrate [J]. Journal of American Ceramic Society, 1999, 82: 1409−1415.

[39] TIAN H, WACHS I E, BRIAND L E. Comparison of UV and visible Raman spectroscopy of bulk metal molybdate and metal vanadate catalysts [J]. Journal of Physical Chemistry B, 2005, 109: 23491−23499.

[40] KUDO A, TSUJI I, KATO H. $AgInZn_7S_9$ solid solution photocatalyst for H_2 evolution from aqueous solutions under visible light irradiation [J]. Chemical Communications, 2002, 17: 1958−1959.

[41] MANIKANDAN A, SRIDHAR R, ANTONY S A, RAMAKRISHNA S. A simple aloe vera plant-extracted microwave and conventional combustion synthesis: Morphological, optical, magnetic and catalytic properties of $CoFe_2O_4$ nanostructures [J]. Journal of Molecular Structure, 2014, 1076: 188−200.

[42] XIE L, MA J, XU G. Preparation of a novel Bi_2MoO_6 flake-like nanophotocatalyst by molten salt method and evaluation for photocatalytic decomposition of rhodamine B [J]. Material Chemistry and Physics, 2008, 110: 197−200.

[43] BELVER C, ADÁN C, FERNÁNDEZ-GARCÍA M. Photocatalytic behaviour of Bi_2MO_6 polymetalates for rhodamine B degradation [J]. Catalysis Today, 2009, 143(3−4): 274−281.

[44] LOPPINI E, ROCHFORD J, CHEN H, SARAF G, LU Y, HAGFELDT A, BOSCHLOO G. Fast electron transport in metal organic vapor deposition grown dye-sensitized ZnO nanorod solar cells [J]. Journal of Physical Chemistry B, 2006, 110: 16159−16161.

[45] LAW M, GREENE L E, JOHNSON J C, SAYKALLY R, YANG P. Nanowire dye-sensitized solar cells [J]. Nature Materials, 2005, 4: 455−459.

[46] HUA G, ZHANG Y, ZHANG J, CAO X, XU W, ZHANG L. Fabrication of ZnO nanowire arrays by cycle growth in surfactantless aqueous solution and their applications on dye-sensitized solar cells [J]. Materials Letters, 2008, 62: 4109−4111.

[47] XU S H, FENG D L, SHANGGUAN W F. Preparations and photocatalytic properties of visible-light-active zinc ferrite-doped TiO_2 photocatalyst [J]. Journal of Physical Chemistry C, 2009, 113: 2463−2467.

[48] MOHAMED R M, AAZAM E. Synthesis and characterization of P-doped TiO_2 thin-films for photocatalytic degradation of butyl benzyl phthalate under visible-light irradiation [J]. Chinese Journal of Catalysis, 2013, 34: 1267−1273.

[49] AHMED S, RASUL M G, MARTENS W N, BROWN R, HASHIB M A. Heterogeneous photocatalytic degradation of phenols in wastewater: A review on current status and developments [J]. Desalination, 2010, 261: 3−18.

溶胶−凝胶法制备 Bi_2MoO_6 纳米光催化剂的结构、形貌和光磁特性

V. UMAPATHY[1,2], A. MANIKANDAN[3], S. ARUL ANTONY[3], P. RAMU[4], P. NEERAJA[5]

1. Research and Development Centre, Bharathiar University, Coimbatore, Tamil Nadu 641 046, India;
2. Caplin Point Laboratories Limited, Chennai 600 017, India;
3. PG and Research Department of Chemistry, Presidency College, Chennai 600 005, India;
4. Department of Chemistry, Meenakshi Academy of Higher Education and Research, Chennai, Tamil Nadu 600 009, India;
5. Department of Chemistry, Adhiyamaan College of Engineering, Hosur, Tamil Nadu 635 109, India

摘　要：采用硝酸铋、钼酸铵、柠檬酸和乙基纤维素为原料，通过溶胶−凝胶法制备钼酸铋(Bi_2MoO_6)纳米颗粒。通过 X 射线衍射(XRD)、傅里叶变换红外光谱(FT-IR)、高分辨扫描电镜(HRSEM)、能谱分析(EDX)、紫外−可见漫散射光谱(DRS)、光致发光光谱(PL)和振动样品磁强计(VSM)等手段对制备的粉末结构、形貌、光磁性和光催化性能进行表征。XRD、 FT-IR 和 EDX 结果表明，制备的粉末是具有斜方晶结构的纯单相晶体 Bi_2MoO_6。HRSEM 图像显示，制备的粉末具有很好的纳米颗粒结构。VSM 结果显示制备的纳米颗粒具有超顺磁性。Bi_2MoO_6 纳米颗粒的光催化活性实验发现 TiO_2 催化剂的添加提高 Bi_2MoO_6 纳米颗粒的光催化活性。催化剂 Bi_2MoO_6、TiO_2 和混合氧化物催化剂 Bi_2MoO_6−TiO_2 纳米复合材料对 4-氯酚的光催化降解(PCD)，发现 Bi_2MoO_6−TiO_2 纳米复合材料的 PCD 效率比纯 Bi_2MoO_6 和 TiO_2 催化剂的 PCD 效率高。

关键词：Bi_2MoO_6；纳米结构；溶胶−凝胶合成法；光学性能；磁性能；光催化剂

(Edited by Mu-lan QIN)